Advances in Science and Technology Research Journal

Advances in Science and Technology Research Journal, 2026, 20(10), 193–204
https://doi.org/10.12913/22998624/224902
ISSN 2299-8624, License CC-BY 4.0

Received: 2026.05.04
Accepted: 2026.07.22
Published: 2026.09.01

Analysis of the influence of laser processing of aluminium-magnesium alloy 5754 on the residual stress state in the surface layer

Barbara Ewa Cecińska[1*], Jacek Mucha[2], Kazimiera Dudek[3]

[1] Department of Manufacturing Processes and Production Engineering, Faculty of Mechanical Engineering and Aeronautics, Rzeszow University of Technology, ul. Powstańców Warszawy 12, 35-029 Rzeszów, Poland

[2] Department of Mechanical Engineering, Faculty of Mechanical Engineering and Aeronautics, Rzeszow University of Technology, ul. Powstańców Warszawy 12, 35-029 Rzeszów, Poland

[3] Institute of Materials Engineering, Faculty of Exact and Technical Sciences, University of Rzeszow, ul. Pigonia 1, 35-310 Rzeszów, Poland

* Corresponding author's e-mail: barbara.ciecinska@prz.edu.pl

ABSTRACT

Laser beam surface treatment of various materials is currently successfully used in various manufacturing processes. This paper presents the results of experimental studies and analyses of the effect of selected parameters of fiber laser treatment of the surface of an EN AW-5754 aluminum alloy. This alloy contains magnesium, chromium, and manganese and is used as a structural material in construction, railways, maritime transport, aviation, mechanical engineering, and other industries. A 1 mm thick sheet was used in the experiment, and the surface was treated with a fiber laser according to eight variants. The variants were differentiated by the number of treatment repetitions (10, 15, and 20 times), pulse frequency (25 and 45 kHz), and beam speed relative to the surface (100 and 200 mm/s). The residual stresses on samples with modified surfaces were measured using an X-ray diffractometer. The results were compared with stresses measured on sandblasted and rolled surfaces. It was found that, unlike with rolling and sandblasting, tensile stresses were formed after laser processing. Laser processing, which results in a relatively repeatable geometric surface structure, influenced the variation of these stress values depending on the directionality of the geometric structure. The results obtained in this way can be used during laser surface processing in cases where the surface structure created by the laser is important. Still, the appropriate direction of the forces acting on the structure must also be selected.

Keywords: residual stress, laser treatment, geometric structure of a surface.

INTRODUCTION

Residual stresses are an inevitable consequence of most material manufacturing and machining processes. They remain after production, even when no external forces are applied to the product [1]. They are a natural consequence of induced non-uniform deformations resulting from thermal gradients during rapid heating and cooling, mechanical operations, and solid-phase transformations [2]. In machining processes, compressive stresses are preferred. They are desirable for improving fatigue strength, fracture toughness, and service life. [3] It has long been recognized that tensile stresses are unfavorable because they promote crack initiation, stress corrosion cracking, and reduce the fatigue life of components [4, 5].

The machining process generates complex stresses as a result of phenomena described by mechanical and thermal models [6]. When considering machining, both models are present, whereas in the case of non-contact machining, only the thermal model is used. The mechanical model assumes the generation of residual stresses as a result of the cutting force alone. Compressive stresses then appear in the surface layer and tensile stresses in the deeper zone [7]. The thermal model assumes the generation of residual stresses solely as a result of temperature, with tensile stresses appearing in the surface layer and compressive stresses deeper in the zone [8]. Paper [9] indicated that friction, high temperature in the cutting zone, plastic deformation, and chip formation are the dominant factors in the generation of stresses during cutting. In such cases, the proper selection of cutting parameters is crucial. Higher cutting speeds and tool wear increase temperature, which in turn leads to higher tensile stresses in the surface layer. In turn, a larger radius of the cutting edge, cooling, as well as causing strong plastic strain favor the formation of compressive stresses [10].

There are also processes that generate favorable compressive stresses in the surface layer, including shot peening. Intensive shot peening significantly increases hardness and generates compressive stresses, improving abrasion resistance, fatigue strength, and affects the homogeneity of the surface layer's microstructure, increasing dislocation density, which translates into increased hardness and improved operational properties [11]. However, as with machining, optimal process parameters are essential. Compressive stresses cause a significant increase in fatigue life, but they can gradually relax under cyclic loading, as observed in the case of the Ti6Al4V titanium alloy in [12]. Studies on the 7075-T6 alloy [13] indicated that the shot peened structure may cause earlier crack initiation. In this case, the presence of compressive stresses delayed crack propagation and contributed to increased fatigue life. In the research conducted by [11] on carburized steel, the possibility of surface damage and reduced durability of the products was found and the optimal intensity of the process was determined.

During laser machining, there is no physical contact between the tool and the machined surface, so the classical mechanical model of residual stress formation does not occur. Laser machining is characterized by extremely high temperature gradients and very short heating and cooling cycles in the laser beam-affected zone, which causes plastic deformation and the formation of a specific stress state. For example, during laser sintering of powders, deformation, cracks, and delamination of sintered layers due to significantly high tensile stresses have been observed [10]. In turn, [14] found that in laser cladding, rapid heating and cooling cause large temperature differences between the substrate and the cladding layer. This leads to significant tensile stresses and the appearance of cracks.

In the context of laser additive manufacturing, key process parameters include laser power, scanning speed, beam diameter, hatch spacing, and scanning strategy. The authors of [10] indicate that during high-power laser melting, the molten material solidifies, and residual stresses occur due to thermal and plastic loading. These can cause effects such as delamination, cracking, and distortion, loss of shape accuracy, and a decrease in fatigue strength. [14] indicates that post-processing stresses can be reduced by prior heat treatment, which induces phase transformations, and [15] by substrate texturing, which reduces the temperature gradient.

Sometimes laser processing causes damage to the surface, as is the case with composites, and then the most important decision is to qualify the product for further production [16].

In the experimental work presented in this article, no prior texturing was planned. The research aims to investigate the effect of laser beam energy on the substrate of samples intended for bonding. Heat treatment or other methods of reducing stress in the substrate were not feasible and were not planned for this experiment. However, laser texturing was selected as an effective and repeatable tool based on the authors' previous work. As demonstrated in the studies described in [17–20], laser processing can produce a repeatable, rough, and sufficiently developed surface that allows for the formation of adhesive joints with high shear strength. Laser processing of surfaces prepared for bonding is of interest to the authors; hence, the specific method of implementing this processing on the sample surfaces. The nature and magnitude of stresses on surfaces prepared for gluing overlaps have not been studied to date in this context.

The research described in this article demonstrated that a compromise is necessary between the tensile stress state established after laser texturing and the desired geometric structure. As with other laser processes, it was determined that optimal processing parameters needed to be established. The influence of laser beam parameters was determined, with the least favorable stress state achieved at a frequency of 45 kHz and a scanning speed of 200 mm/s. Furthermore, increasing the processing intensity through a greater number of passes is not beneficial. For a gap spacing of 0.125 mm, a compressive stress state was achieved, but this processing variant involved prolonged exposure to heat on the surface. This may be important when joining thin-walled components due to possible surface deformation.

EXPERIMENTAL RESEARCH

Material and sample preparation

EN AW-5754 aluminum alloy with a composition consistent with [21] and given in Table 1 was used for the tests. Samples with dimensions of 25 × 100 mm were made by cutting them out of 1 mm thick sheet metal with a guillotine.

The geometric structure and residual stresses were examined on a surface created at the planned lap joint for bonding a single-lap joint measuring 25 × 12.5 mm (Figure 1). The lap surfaces were laser-processed with various parameter configurations. A G3 laser from SPI (TRUMPF Group) was used for the tests, running on Galvo Laser Marking Software from DK Lasertechnik, Kraków, Poland. This is an air-cooled, single-mode ytterbium fiber laser with a wavelength of 1030–1200 nm and a power of 20 W. The pulse duration is 200 ns, and the spot size is approximately 2 µm. The laser power is adjustable from 1 to 100%, the scanning speed ranges from 1 to 10.000 mm/s, and the pulse frequency ranges from 2 to 1.000 kHz. The spacing between tracks is defined in the program via a graphical interface.

For comparison purposes, samples were also made with surfaces:
- rolled in the H22 delivery condition (hardened by rolling and partially annealed to ¼ hardness)
- blasted with F280 electro corundum in an ejector chamber, with the nozzle positioned 100 mm from the sample surface and inclined at a 45° angle to it, with an operating pressure of 0.3 MPa.

The options of the overlap surface treatment are given in Table 2.

Additionally, variant E with a laser path spacing of 0.5 mm was compared with a surface made by laser with the same parameters but with a spacing of 0.25 and 0.125 mm (Table 3).

Table 1. Chemical composition of the EN AW-5754 aluminum alloy [21]

Element	%	Element	%	Element	%
Mg	2.666	Cu	-	Si + Fe	0.417
Mn	0.261	Zn	0.001	Mn + Cr	0.289
Fe	0.194	Cr	0.028	Other all	0.037
Si	0.223	Ti	0.020	Al	rest

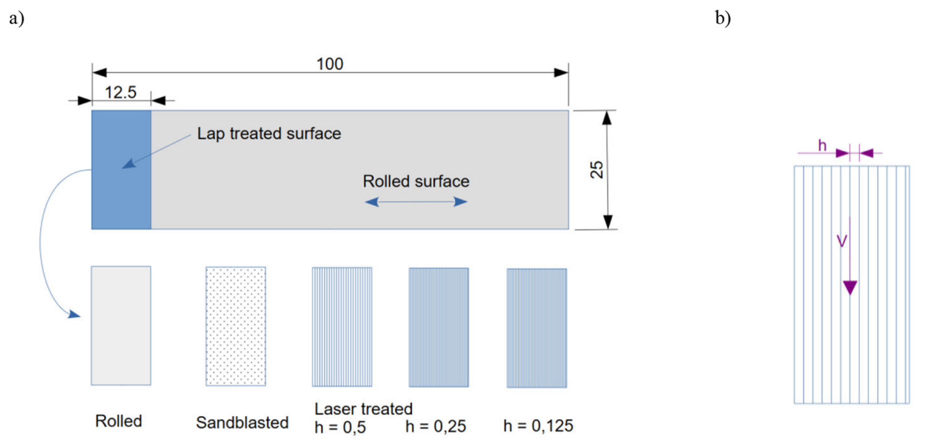

Figure 1. Scheme of lap treatment: a) all options – rolled, sandblasted and laser treated (h – distance between laser path, mm), b) hatch and laser path location (v – scanning speed of laser beam)

Table 2. Options of lap surface treatment

Sample mark	Number of repetitions	Speed of scanning V, mm/s	Power of laser, P, W	Impulse frequency F, kHz	Distance between laser path h, mm
A	10	200	20	45	0.5
B	15	200		45	0.5
C	20	200		45	0.5
D	20	100		45	0.5
E (E1)	20	100		25	0.5
F	20	200		25	0.5
S			Sandblasting with electro corundum F280 use of grain size 45±4 µm, air pressure 0.3 MPa, nozzle distance to sample 100 mm, tilt angle 45°		
R			Rolling according to the direction shown in Figure 1		

Table 3. Option of E samples

Sample mark	Number of repetitions	Speed of scanning V, mm/s	Power of laser P, W	Impulse frequency F, kHz	Distance between laser path h, mm
E1	20	100	20	25	0.5
E2					0.25
E3					0.125

The selection of parameters such as those in Tables 2 and 3 is correlated with the authors' other studies. In the context of effective surface texturing and imparting a specific geometric structure to it, a set of laser parameters was sought that would allow for obtaining a joint with the possible highest shear strength after bonding. In the earlier studies, the textured surfaces of the lap were compared to the surfaces after rolling and sandblasting using the parameters given here. Separate studies on the shear strength of joints demonstrated that the peaks and valleys created by the laser beam play a significant role. These studies were conducted with some of the parameters given in Table 2. The height of the peaks, the depth of the valleys, and the surface development were then shown to be significant, but the residual stress state was not examined. In this article, Tables 2 and 3 provide a set of combinations of laser parameters to provide a broader view of their impact on the surface layer.

Study of the geometric structure of the surface and the state of residual stress

Identification of selected surface topography parameters for the studied surface preparation cases was performed using a 3D Taylor Hobson Talyscan 150 Laser Scanner (Taylor Hobson, Leicester, UK). Residual stress measurements were performed using an XSTRESS 3000 G3R diffractometer and XTronic v.1.6.1 control software from Stresstech Oy (Finland) (Figure 2) using the X-ray method.

This is a non-destructive method used for crystalline materials, including the tested alloy EN AW-5754. The residual stress measurement procedure included calibration to determine the collimator distance, i.e., the distance between the collimator tip and the surface of the tested element. A standard powder sample (the stress-free powder sample A1, PW62, Figure 3) was used in the calibration process, representing a model of the tested material.

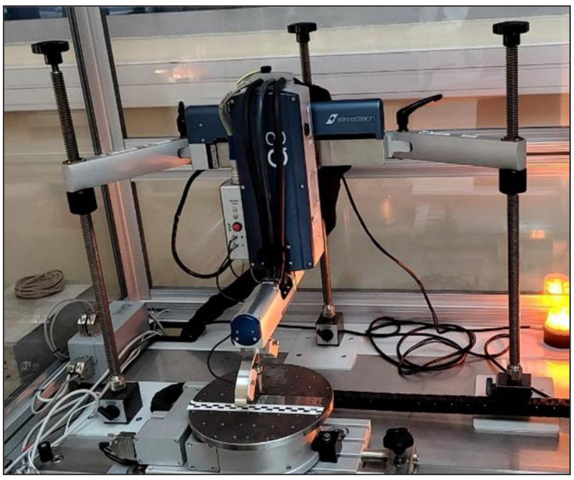

Figure 2. X-ray diffractometer used in the research

Figure 3. The stress free powder sample A1, PW62

For EN AW-5754, the diffraction angle 2θ was assumed to be 139.3°. According to the calibration results (Figure 4), a distance of 16.49 mm was assumed for each of the tested processing variants. A collimator with a diameter of 3 mm was selected so that the X-ray beam covered the measurement area and the varied surface texture of the tested elements.

The number of tilts of the ψ angle at which the lattice constant d was measured – the measurement procedure for the fixed exposure time of 10 s each included taking lattice constant measurements perpendicular to the surface of the tested sample (angle ψ = 0° on the positive and negative tilt sides) and at four other values of the ψ angle, specified in detail in Table 4, in the range of +45° (positive tilt side) and -45° (negative tilt side). The value of the ψ angle resulted from the "Auto" division mode (tilt angles are calculated in equal intervals on the sin2ψ scale) [22]. The schematic diagram illustrating the method of measurement is shown in the Figure 5.

For the calculations, the Poisson ratio of the tested alloy was assumed to be 0.33, and the Young Modulus E was 70500 MPa, and the sin2ψ method based on Bragg's law was used. In this method, the stress value in the tested direction is determined from the relationship [23]:

$$\sigma_\varphi = \frac{E}{(1+\nu)\,sin^2\,\psi}\left(\frac{d_\psi - d_n}{d_n}\right) \tag{1}$$

where: E – Young modulus, ν – Poisson ratio, d_ψ – value of the lattice constant measured at angle ψ, dn – lattice constant measured for zero tilt ($\psi = 0°$) when the X-ray beam is incident perpendicularly to the surface.

Table 4. Assumed angle values ψ

No. of tilt	Negative ψ tilts	Positive tilts ψ
1	0	0,0
2	-20,7°	20,7°
3	-30°	30°
4	-37,8°	37,8°
5	-45°	45°

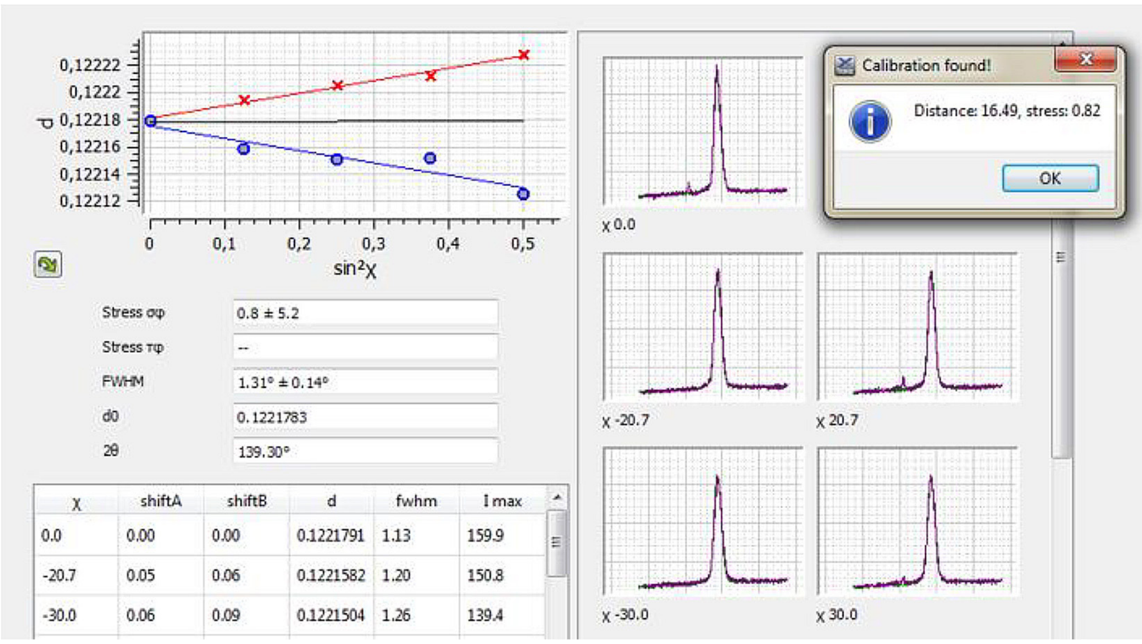

Figure 4. Calibration results

Theoretically, to determine the stress in the φ direction, at least two measurements of the lattice constant d should be performed (at an angle of 0° and any other angle). In the experiment, measurements were performed at 4 measurement points shown in Figure 6a.

For each of the tested samples, four measurement points were determined (Figure 6a). At each measurement point, stresses were measured in two mutually perpendicular directions (φ) designated as "$\varphi_1 = 0°$" and "$\varphi_2 = 90°$" (Figure 6b). For the laser-processed samples, φ_1 was the direction perpendicular to the laser paths, while φ_2 was the direction consistent with the laser paths.

Additional detailed parameters of residual stress measurements are given in Table 5.

RESULTS

The geometric structure of the measurement surface of 4 × 4 mm of the tested rolled, sandblasted, and laser-made samples in variants A-F, as well as in variant E with different distances between the laser beam paths, is shown in Figure 7.

The values of the measured parameters describing the geometric structure are given in Table 6.

In the tests of residual stresses based on measurements at four points, the results given in Table 7 were obtained.

Table 5. Diffractometric measurement parameters

Measurement parameters		Value
Calculations	2theta (2*θ*)	Calibration
	Background subtraction	Linear
	Used detectors	A and B
	Peak limiting	lack
	Peak shift	Cross correlation
Material data	Material	EN-AW 5754
	Characteristic diffraction angle	139,3°
	Young modulus	70 500 MPa
	Poisson's ratio, *v*	0.33
Measurement parameters	2*θ*/hkl	139.3°/311
	Exposure time	10 s
	Method	Psi (y)
	φ / Oscillations φ	0°; 90° / lack
	ψ / Oscillations ψ	5/5; - 45°/45° / lack
	X-ray tube	Cr

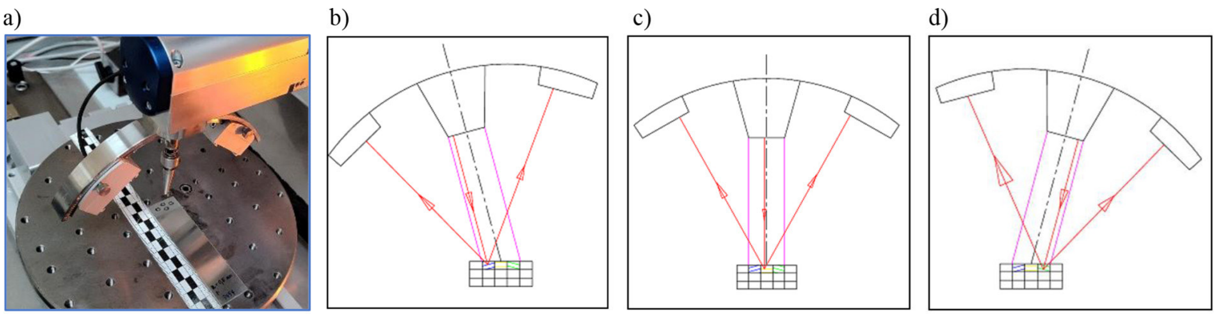

Figure 5. Schematic diagram illustrating the method of performing the residual stress test: a) sample view, b) diffraction on negative inclination ψ, c) without inclination ψ = 0° (no inclination), d) diffraction on positive inclination ψ [(a) own photography, (b-d) [22]

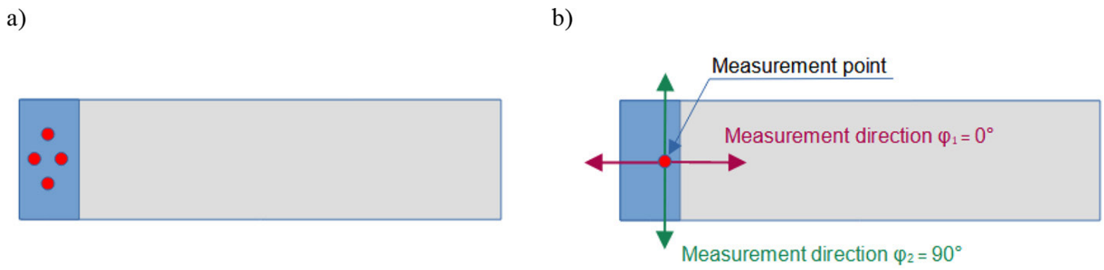

Figure 6. Location of measurement points on the sample (a), directions of stress measurement for a single measurement point φ (b)

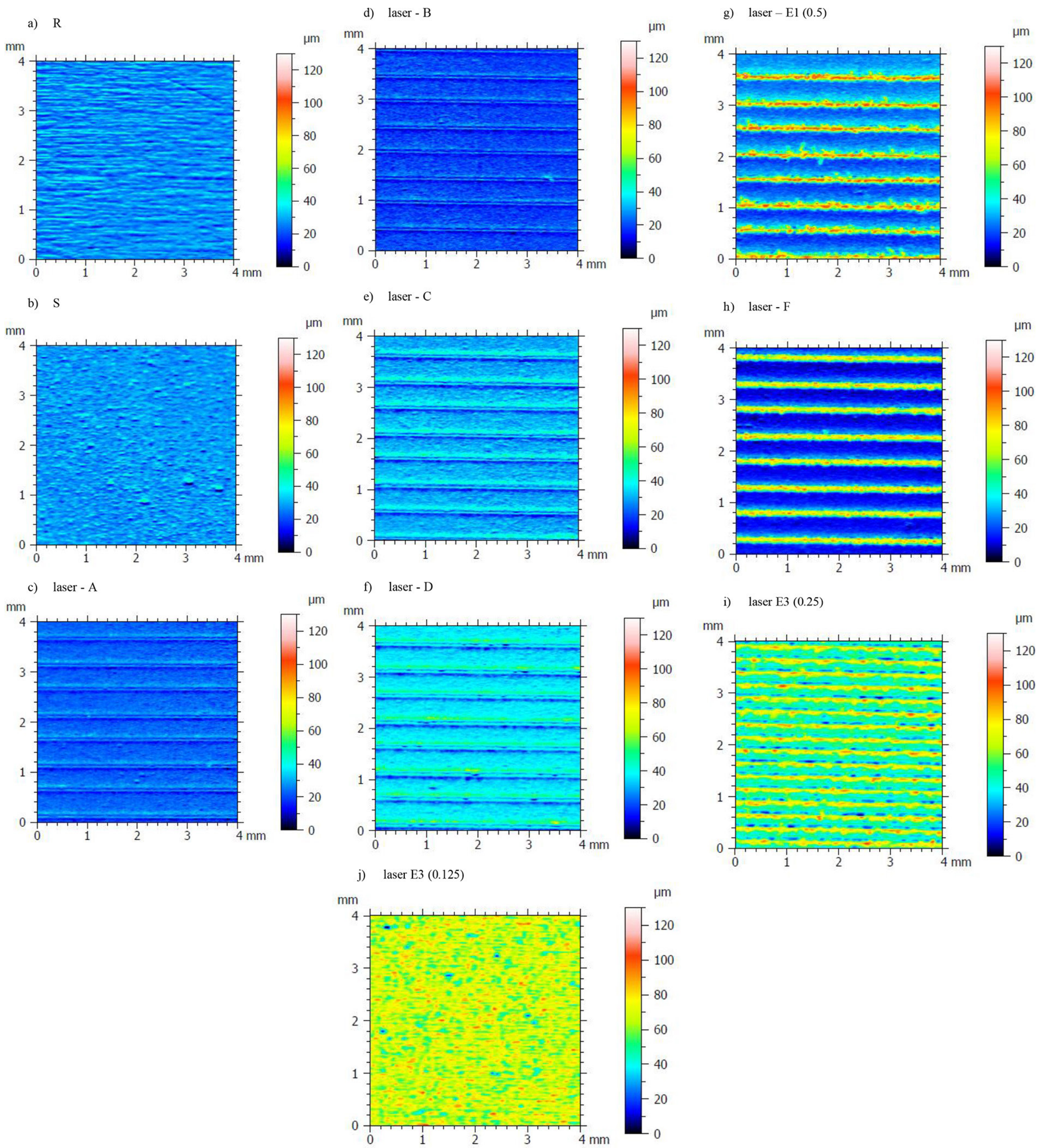

Figure 7. Geometrical structure of samples R, S, A÷F of h=0.5 and E2 of h=0.25 and E3 of h=0.125 mm

Analysis of results

The rolled and sandblasted surfaces were characterized by compressive stresses in both measurement directions. Laser processing transformed this state into tensile stresses, varying in magnitude depending on the measurement direction and, simultaneously, the directionality of the surface structure after laser processing. The Sz parameter, reflecting the actual scale of surface unevenness change, was used to relate the stress state to the structure created by the laser beam, while the Sdr parameter was used to assess the surface's suitability for gluing.

Increasing the laser processing intensity and the beam's exposure time on the surface resulted in a reduction of tensile stresses in the 0° direction (perpendicular to the machining marks) (Figure 7c, 7e, and Figure 8). Machining with 20 repetitions is associated with stresses of approximately 33.3 MPa, which, compared to variant A, i.e., machining with 10 repetitions and stresses of approximately 43.7 MPa, represents a decrease of approximately 23.8%. However, tensile stresses

Table 6. Measurement results of selected geometric structure parameters

Parameter	Options of surface treatment				
	R	S	A	B	C
Sa, µm	3.027	4.613	3.088	3.439	4.956
Sq, µm	4.043	5.765	4.060	4.441	6.522
Sp, µm	24.28	21.41	17.10	24.99	22.89
Sv, µm	28.16	27.11	22.39	19.39	24.93
Sz, µm	52.34	48.52	39.49	44.38	47.81
Sal, mm	0.02231	0.01969	0.0335	0.02197	0.04945
Sdq, -	0.3284	0.4771	0.3262	0.4160	0.4166
Sdr, %	4.957	10.020	4.907	7.730	7.669

Note: Sa – arithmetic mean surface deviation, µm; Sq – mean square deviation of the surface, µm; Sp – maximum elevation, µm; Sv – maximum value of cavities, µm; Sz – maximum surface height, the sum of the highest elevations and lowest cavities, µm; Sal – autocorrelation length, describes the dominant size of the surface structure elements, mm; Sdg – average surface tilt; Sdr – surface development index, increase in actual surface area compared to nominal surface area, %.

Table 7. Mean stress values and standard deviation

Surface treatment options	Stresses measured in the direction 0°, MPa	δ	Stresses measured in the direction 90°, MPa	δ
R	-16.125	9.065	-22.625	9.581
S	-111.875	3.476	-107.850	0.681
A	43.725	12.791	25.000	8.636
B	41.100	17.946	25.233	17.666
C	33.300	6.053	30.600	6.292
D	24.600	7.973	21.575	9.133
E1 (0.5)	15.625	14.531	25.950	6.435
E2 (0.25)	5.250	5.378	32.075	7.465
E3 (0.0125)	-50.733	10.356	36.850	4.337
F	25.875	9.162	15.825	5.172

in the measurement direction consistent with the machining direction (90°) increase from 25.0 MPa (variant A) to 30.6 MPa, which is a 22.4% increase. The increase in tensile stress values in this direction is also associated with an increase in surface roughness, from Sz = 39.49 to 47.81 µm. Moreover, the surface becomes slightly more developed with the increase in the number of beam pass repetitions, as evidenced by the increase in the Sdr parameter from 4.9 to 7.7%.

Increasing the laser pulse frequency from 25 to 45 kHz caused an increase in the tensile stress value in the direction perpendicular to the machining marks (measured in the 0° direction) from 15.6 to 24.6 MPa, which is an increase of approximately 57%. Stresses measured in the direction consistent with the grooves formed after machining (90°) decreased from 25,950 to 21,575 MPa (by approximately 16.8%). With the decrease in value, the surface roughness also decreased: Sz was 128.9 µm and decreased to 71.6 µm, respectively, which constituted a decrease of approximately 44.5%. At the same time, the degree of surface development decreased threefold, the Sdr value dropped from 15.9% to approximately 5% (Figure 7g, 7f and Figure 9).

In turn, increasing the surface scanning speed with a laser beam with a pulse frequency of 45 kHz caused an increase in the tensile stress values in both measurement directions. In the 0° direction (perpendicular to the direction of the machining marks), the stresses increased by approximately 35% (from 24.6 to 33.3 MPa), and in the 90° direction (along the machining marks) by approximately 42% (from 21.575 to 30.6 MPa). With increasing speed, the surface roughness Sz decreased from 71.6 to 47.81 µm, and the degree of surface development Sdr increased by

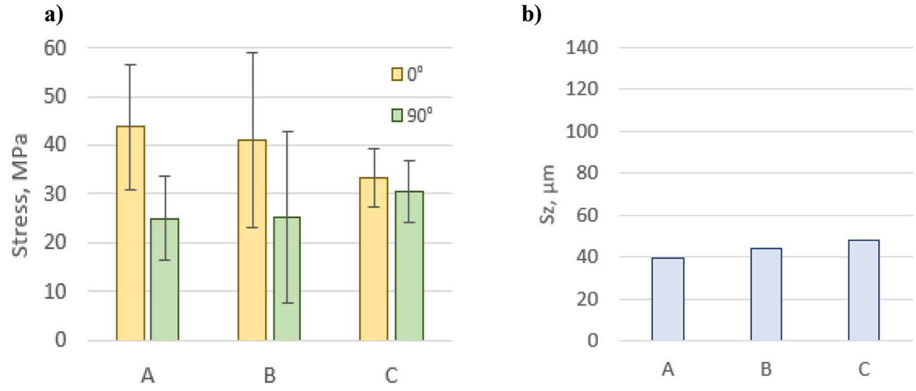

Figure 8. Comparison of the effect of the number of repetitions – A (10x), B (15x), C (20x): a) on the stress state on the surface, b) on the surface roughness Sz

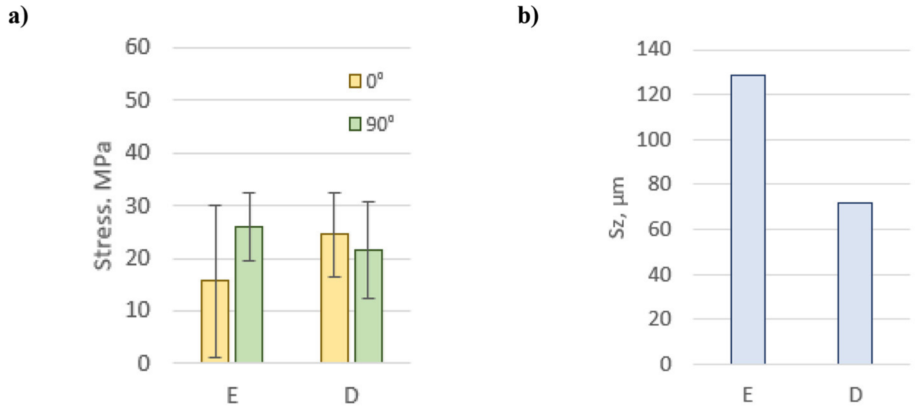

Figure 9. Comparison of the impact of pulse frequencies E (25 kHz) and D (45 kHz): a) on the stress state on the surface, b) on the surface roughness Sz

approximately 50%, although it was still small (from 5.029 to 7.669%) (Figure 7f, 7e and 10).

Machining with increasing speed but lower frequency (25 kHz) resulted in changes of a slightly different nature than those described above. Only the value of stresses measured in the 0° direction increased (from 15.625 to 25.875 MPa, which is ca. 65.6%), while in the 90° direction it decreased, from 25.959 to 15.825 MPa (ca. 39%). The increase in speed at lower frequency also caused a slight decrease in surface roughness Sz from 128.9 to 120.4 µm

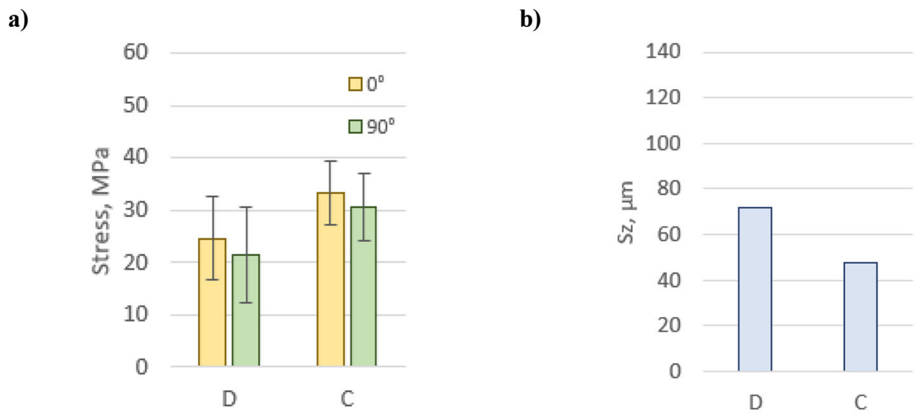

Figure 10. Comparison of the effect of scanning speed D (100 mm/s) and C (200 mm/s) for 45 kHz: a) on the stress state on the surface, b) on the surface roughness S

and in its degree of development from 15.9 to 13.59% (Figure 7g, 7h and 11).

The effect of changing the distance between the laser beam paths was also investigated. It was found that by densifying the machining marks (Figure 7g, 7i and 7j), the machining intensity increased, which simultaneously translated into an increase in the stress value in the 90° direction to 36.85 MPa (Figure 12). However, in contrast to the previously described variants, the stresses at the smallest distance h=0.125 mm between the laser paths changed their nature from tensile to compressive (50.733 MPa). The surface roughness Sz slightly decreases with decreasing distance h, and the degree of surface development Sdr slightly increases at h=0.25 mm (from 15.9% for E1 to 16.93 for E2), but decreases at h=125 mm (to 12.52%).

Increasing the processing intensity by densifying the laser beam paths resulted in the deformation of the tested samples shown in Figure 13.

This may be a significant obstacle to the use of such machining parameters in the context of

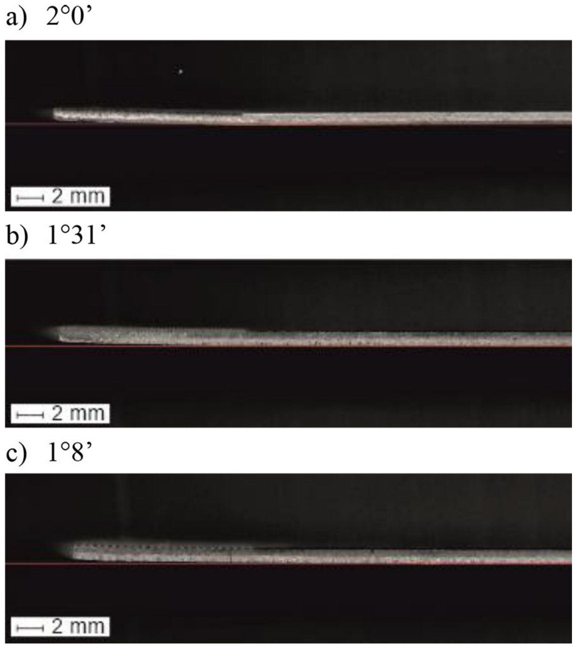

Figure 13. Appearance of the sample and the value of the sample deformation angle resulting from the adopted hatch spacing: a) 0.125 mm, b) 0.25 mm, c) 0.5 mm

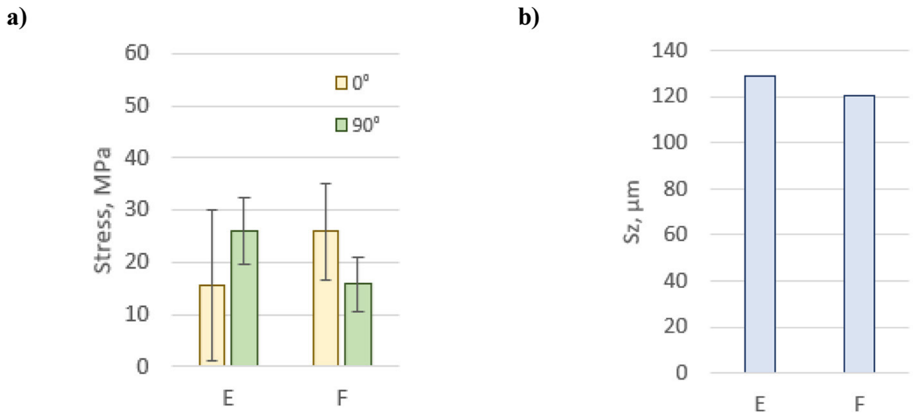

Figure 11. Comparison of the effect of scanning speed E (100 mm/s) and F (200 mm/s) for 25 kHz: a) on the stress state on the surface, b) on the surface roughness Sz

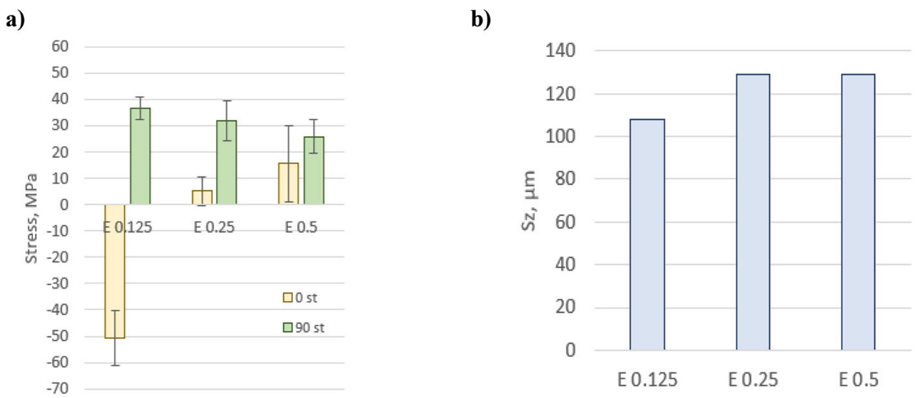

Figure 12. Comparison of the influence of the distance h between the laser beam paths for 25 kHz E (0.5 mm), E2 (0.25 mm) and E3 (0.125 mm): a) on the stress state on the surface, b) on the surface roughness Sz

further machining operations in the manufacturing or assembly process.

CONCLUSIONS

From literature reviews and analysis of results, it is known that laser processing induces tensile stresses on the surface. However, in the presented studies, where it is used in the context of surface preparation before bonding, the processing is not very intensive and generates stresses significantly lower than those resulting from processing involving melting the surface layer.

The authors' previous research indicates that laser processing is highly beneficial, producing adhesive joints with high shear strength. Laser processing can also be recommended due to the superior strength of laser-labeled joints compared to sandblasted joints, which provides a basis for eliminating the more cumbersome production method (noise, contamination, waste, automation issues, repeatability, etc.). The creation of tensile stresses necessitates consideration of the directionality of laser processing relative to the direction and nature of forces acting on the adhesive joint during operation. In most of the presented comparisons, the preferred option is to design the beam paths perpendicular to the direction of the shearing force.

The stress state on the surface was related to the geometric structure and its degree of development. The specific surface roughness and development significantly influence the mechanical adhesion conditions and bonding results. Despite tensile stresses, the laser can produce a surface that is much rougher compared to sandblasting (Sz = 128.9 µm with the laser in variant E1 compared to Sz = 48.52 µm after sandblasting), as well as more developed (Sdr after laser was 15.9%, and after sandblasting 10.02%). Such surface conditions may contribute to the choice of laser processing despite the unfavorable stress state on the surface.

In examining the state of surface stresses related to the geometric structure of the surface, a characteristic feature can be identified, resulting from the adopted laser processing parameters. A predetermined spacing of h between the beam paths was assumed, leaving spaces undeformed by the beam energy after processing. As the distances decrease, the nature of the stresses changes. The closer the paths are to each other, the more favorable the stresses. In variant E3, where processing effects are cumulative, the geometric structure begins to resemble a sandblasted structure, and the stresses are compressive in the direction of the forces that would break the potential adhesive bond. This suggests that it is possible to create good adhesion conditions while simultaneously maintaining favorable surface stresses in the joint.

Analyzing the standard deviation values, it can be concluded that rolled and sandblasted surfaces are characterized by high repeatability of the considered structural parameters and stresses. Stress measurements on laser-processed surfaces should be performed with the homogeneity of the structure taken into account. In the presented experiment, the surfaces did not have a homogeneous structure due to the adopted distance h between the laser paths, which could have caused the higher standard deviation values. In the future, if a specific geometric structure is important, stress measurements could be made using a smaller diameter X-ray diffractometer collimator, if possible, or measurements could be made at specific locations on the surface, e.g., bypassing areas unaffected by the laser.

REFERENCES

1. Tabatabaeian A., Ghasemi A.R., Shokrieh M.M., Marzbanrad B., Baraheni M., Fotouhi M. Residual stress in engineering materials: A review. Adv Eng Mater. 2022;24(3):2100786. https://doi.org/10.1002/adem.202100786
2. Chen S.G., Gao H.J., Zhang Y.D., Wu Q., Gao Z.H., Zhou X. Review on residual stresses in metal additive manufacturing: formation mechanisms, parameter dependencies, prediction and control approaches. J Mater Res Technol. 2022;17:2950–2974. https://doi.org/10.1016/j.jmrt.2022.02.054
3. Vergara D., Fernández-Arias P., Ariza-Echeverri E.A., del Bosque A. Residual stresses in metal manufacturing: a bibliometric review. Materials (Basel). 2025;18:3612. https://doi.org/10.3390/ma18153612
4. Matsumoto Y., Magda D., Hoeppner D.W., Kim T.Y. Effect of machining processes on the fatigue strength of hardened AISI 4340 steel. J Eng Mater Technol. 1991;113(3):235–240. https://doi.org/10.1115/1.2899672
5. Sasahara H. The effect on fatigue life of residual stress and surface hardness resulting from different cutting conditions of 0.45% C steel. Int J Mach Tools Manuf. 2005;45(2):131–136. https://doi.org/10.1016/j.ijmachtools.2004.08.002

6. Zawada-Michałowska M., Pieśko P., Korpysa J. Study of the relationship between milling conditions and residual stresses in the surface layer of aircraft aluminum alloys. In: Eng. 17th Scientific and Technical Conference TKI 2024 – Computer Techniques in Engineering; 15–18 Oct 2024; Poland.
7. Weber D., Kirsch B., Chighizola C.R., D'Elia C.R., Linke B.S., Hill M.R., Aurich J.C. Analysis of machining-induced residual stresses of milled aluminum workpieces, their repeatability, and their resulting distortion. Int J Adv Manuf Technol. 2021;115(4):1089–1110. https://doi.org/10.1007/s00170-021-07171-7 [eprints.gla.ac.uk]
8. Zawada-Michałowska M., Pieśko P., Mrówka-Nowotnik G., Nowotnik A., Legutko S. Effect of the technological parameters of milling on residual stress in the surface layer of thin-walled plates. Materials (Basel). 2024;17(5):1193. https://doi.org/10.3390/ma17051193
9. Soori M., Arezoo B. A review in machining-induced residual stress. J New Technol Mater. 2022;12(1):64–83.
10. Kazemi Movahed A., Ghanavati R., Saboori A., Iuliano L. A review of strategies for in situ mitigating of residual stress in laser-based metal additive manufacturing: insights, innovations, and challenges. Acta Metall Sin (Engl Lett). 2025;38:1657–1698. https://doi.org/10.1007/s40195-025-01902-5
11. Chen W., Xu Z., Gu X., Gu J., Chi H., Wang B., Zhang P., Zhang Z. Effect of shot peening treatment on rotating bending fatigue performance of high-strength carburized gear steel. Heat Treat Met. 2026;51(1):279–287. https://doi.org/10.13251/j.issn.0254-6051.2026.01.043
12. Zhang H., Cai Z., Chi J., Sun R., Che Z., Zhang H., Guo W. Fatigue crack growth in residual stress fields of laser shock peened Ti6Al4V titanium alloy. J Alloys Compd. 2021;887:161427. https://doi.org/10.1016/j.jallcom.2021.161427
13. Benedetti M., Fontanari V., Rustighi E., Gallo P., Bandini M. Fatigue damage in shot-peened Al7075-T6 alloy: correlation between acoustic emission spectra and fractographic analysis. Metals (Basel). 2026;16(3):346.
14. Jing Z., Xu P., Liu Q., Yu C. Residual stress release during laser cladding process: a review. J Laser Appl. 2023;35(3):032018. https://doi.org/10.2351/7.0000971
15. Zhao C., Ma C., Du W., Yu Z., Zhang Z. Study on the reduction of residual stress in laser cladding layers through groove texture. Sci Rep. 2024;14:15911. https://doi.org/10.1038/s41598-024-65911-9
16. Kłonica M., Kubit A., Perłowski R., Bielawski R., Woś S. Selected methods of modifying the surface layer of a carbon composite. Advances in Science and Technology Research Journal. 2024. https://doi.org/10.12913/22998624/183101
17. Miecińska B. Experimental studies of the possibility of laser processing as a cleaner method of achieving a surface with good adhesion. Prod Eng Arch. 2022;28(3):233–240.
18. Miecińska B., Mucha J., Bąk Ł. Analysis of the effect of surface preparation of aluminum alloy sheets on the load-bearing capacity and failure energy of an epoxy-bonded adhesive joint. Materials (Basel). 2024;17(9):2123. https://doi.org/10.3390/ma17092123
19. Mucha J., Miecińska B. Comparative studies of the geometric structure of the surface of aluminium alloys in the context of adhesive joints with Araldite 2014-2 adhesive. Appl Surf Sci. 2025;709:150395. https://doi.org/10.1016/j.apsusc.2024.150395
20. Miecińska B., Mucha J. Experimental analysis of the impact of selected laser processing parameters on wettability and surface free energy of EN AW-2024 and EN AW-5083 aluminum alloys. Adv Sci Technol Res J. 2025;19(2):179–191. https://doi.org/10.12913/22998624/188941
21. European Committee for Standardization. EN 573-1:2006 Aluminium and aluminium alloys – Chemical composition and form of wrought products – Part 1: Numerical designation system. Warsaw: Polish Committee for Standardization; 2006.
22. Stresstech Oy. Technical manual V.1.0d – Xstress 3000 G3 X-ray Stress Analyzer. Jyväskylä (Finland): Stresstech Oy; 2008.
23. Fitzpatrick M.E., Fry A.T., Holdway P., Kandil F.A., Shackleton J., Suominen L. Determination of residual stresses by X-ray diffraction. Issue 2. National Measurement Good Practice Guide No. 52. Teddington (UK): National Physical Laboratory; 2005; 11–40.